Research in Pharmaceutical Sciences, June 2020; 15(3): 249-262
Received: 15-09-2019
Peer Reviewed: 02-01-2020
Revised: 05-01-2020
Accepted: 07-01-2020
Published: 03-07-2020

School of Pharmacy & Pharmaceutical Sciences
Isfahan University of Medical Sciences

Original Article

Monastrol derivatives: *in silico* and *in vitro* cytotoxicity assessments

Zahra Bidram[1], Hajar Sirous[2], Ghadam Ali Khodarahmi[1,3], Farshid Hassanzadeh[1], Nasim Dana[4], Amir Ali Hariri[1], and Mahboubeh Rostami[1,3,*]

[1]Department of Medicinal Chemistry, School of Pharmacy and Pharmaceutical Sciences, Isfahan University of Medical Sciences, Isfahan, I.R. Iran.
[2]Bioinformatics Research Center, School of Pharmacy and Pharmaceutical Sciences, Isfahan University of Medical Sciences, Isfahan, I.R. Iran.
[3]Pharmaceutical Science Research Center, School of Pharmacy and Pharmaceutical Sciences, Isfahan University of Medical Sciences, Isfahan, I.R. Iran.
[4]Applied Physiology Research Center, Cardiovascular Research Institute, Isfahan University of Medical Sciences, Isfahan, I.R. Iran.

Abstract

Background and purpose: Cancer is the leading cause of death in today's world, therefore the efforts to achieve anticancer drugs with higher potency and fewer side effects have always been conducted by researchers in the field of pharmaceutical chemistry.
Monastrol, a cytotoxic small molecule, from dihydropyrimidinone scaffold, is an inhibitor of the kinesin-5 protein. So, efforts to identify more derivatives of this molecule have been of interest.
Experimental approach: Some of monastrol's analogs as Eg5 inhibitors with different substitution patterns were analyzed, synthesized, and their cytotoxic effects were evaluated on MCF-7 and HeLa cancerous cells *in vitro* using the MTT assay. The structure-activity relationship (SAR) was studied *in silico* by molecular docking.
Findings / Results: Among all proposed structures, in ducking study, those with hydrophobic moieties on the C2-N3 region, those with a hydroxyl group on the phenyl on C4 position, and those with a carboxylic group on C5 were the best candidates. *In vitro* studies, on the other side, emphasized that monastrol still was the most potent derivative. Another finding was the more moderate activity of synthesized compounds on the HeLa cell compared to the MCF-7 cell line. During different challenges for substitution at 5-position, some earlier reports around the dihydropyrimidinone reactions were questioned. It seems that the change at the position 5 is not merely accessible, as earlier reports claimed. Also, we could not achieve any better cell cytotoxicity by the larger group in the thiourea region or position 5; nonetheless, it seems that the introduction of a methylene group at this position could be beneficial.
Conclusion and implications: The initial results of this study were valuable in terms of design and synthesis and will be useful for future investigations.

Keywords: Dihydropyrimidinones; Eg5 inhibitor; *in vitro* cytotoxicity; Molecular ducking; Monastrol.

INTRODUCTION

The biological activity of multi-potential dihydropyrimidinones compounds, their synthesis, and their related reactions have been always an interesting era in chemistry and medicinal chemistry field during the last decades (1-4). After the discovery of monastrol as an efficient inhibitor of kinesin-5 (KIF11 or kinesin Eg5) from this family, it has been the core of attention in several kinds of cancer research (5). Many efforts have been made to design and discover the more potent inhibitors of this family, or to expand the library for high throughput screening in biological projects (6-8).

*Corresponding author: M. Rostami
Tel: +98-9131154200, Fax: +98-*3136680011*
Email: m.rostami@pharm.mui.ac.ir

Access this article online

Website: http://rps.mui.ac.ir

DOI: 10.4103/1735-5362.288427

The most studied mechanism by which monastrol disrupts cell cycle is allosteric inhibition of microtubule-stimulated ADP release from Eg5 (kinesin spindle protein presents in *Xenopus laevis*), followed by apoptotic signaling pathway which leads to efficient cell death. Based on attempts in developing structure-activity relationship (SAR) for Eg5 inhibitors, thione derivatives of dihydropyrimidinones are more potent than oxo ones, and the presence of hydroxyl group in 3' position, make the molecules more potent than those having none, or with the other substitutes (9,10). Since different parts of a molecule interact differentially with the active site residues, which leads to the optimized binding energies, therefore, the accurate analysis of the enzyme active site enables us to design and synthesis more potent dihydropyrimidinones rather than monastrol. In this work, we tried to evaluate how the structural changes affect the cytotoxicity of some monastrols' analogs. At first, we studied these changes *in silico*, and then we synthesized the monastrol's analogs to evaluate cytotoxicity profile *in vitro* on MCF-7 and HeLa cell lines.

MATERIAL AND METHODS

Materials

All of the materials and solvents were supplied commercially and used without further purification. 1-Ethyl-3-(3dimethylaminopropyl) carbodiimide (EDC), hydroxy benzotriazole (HOBt), and anhydrous dimethylformamide (DMF) were purchased from Merck (Germany) and 3-[4,5-dimethylthiazol-2-yl]-2,5-diphenyl tetrazolium bromide (MTT) from Sigma (USA). The RPMI-1640 culture medium was from PAA (Austria). The MCF-7 and HeLa cell lines were supplied by the Pasteur Institute of Iran. Reactions were monitored by thin layer chromatography (TLC) on pre-coated plates of kieselgel 60 F254, which purchased from Merck (Germany), and the spots were detected by exposing the dry plates to UV lamp at 254 nm. We obtained the melting points in open capillaries on a capillary melting point apparatus (Electrothermal 9200 UK), and the data were uncorrected. Proton nuclear magnetic resonance (^{1}HNMR) and carbon-13 nuclear magnetic resonance (^{13}CNMR) spectra were recorded by NMR spectrophotometer (400 MHz, AC-80, Bruker Biospin, Germany) in deuterated dimethyl sulfoxide (DMSO-d_6) and $CDCl_3$ as solvents. Chemical shifts δ were reported in parts per million downfield from tetramethylsilane. Infrared spectra (IR) were recorded on Rayleigh, WQF-510/520, spectrophotometer (China), using KBr disc, and the results were reported in cm^{-1}.

Docking procedure

Molecular docking of thirteen proposed compounds (Fig. 1) with Eg5 binding pocket was analyzed using protein-ligand docking (11). For this purpose, the crystal structure of the kinesin Eg5 in complex with monastrol (protein data bank (PDB) ID: 1Q0B) was retrieved from the PDB. The co-crystallized monastrol, and all of the irrelevant compartments were removed using Accelrys DS visualizer *3.5 (*Studio D, Insight I. Accelrys Software Inc. San Diego, CA 2009; 92121) (12). All missing parts of the active site were merged to their proper places using AutoDock tools (13). For ligand preparation, all structures were drawn and optimized by the MM+ force field and PM3 semi-empirical techniques with the aid of Hyperchem software (Hyperchem, molecular modeling system. Hypercube, Inc., and Auto Desk, Inc.). The partial charges of atoms were calculated using the Gasteiger-Marsili procedure (13). Polar hydrogen atoms of the compounds were added while nonpolar hydrogens were merged. In all dockings, a grid map of 60 × 60 × 60 points with 0.375 Å spacing between grid points was applied. Since the position of the co-crystallized monastrol within the binding site of Eg5 was known, we centered the grid box at the centroid of bounded monastrol in the active site (grid box center coordinate: X: 41.501; Y: 15.727; Z: 48.857), so that roughly encompasses the center of the Eg5 binding pocket. For each ligand, 100 independent docking runs were carried out employing the Lamarckian genetic algorithm (LGA) (11). The factors for LGA were defined as follows: a maximum number of 2.5 × 106 energy evaluations; a maximum number of generations of 27000; mutation and crossover rates of 0.02 and 0.8, respectively.

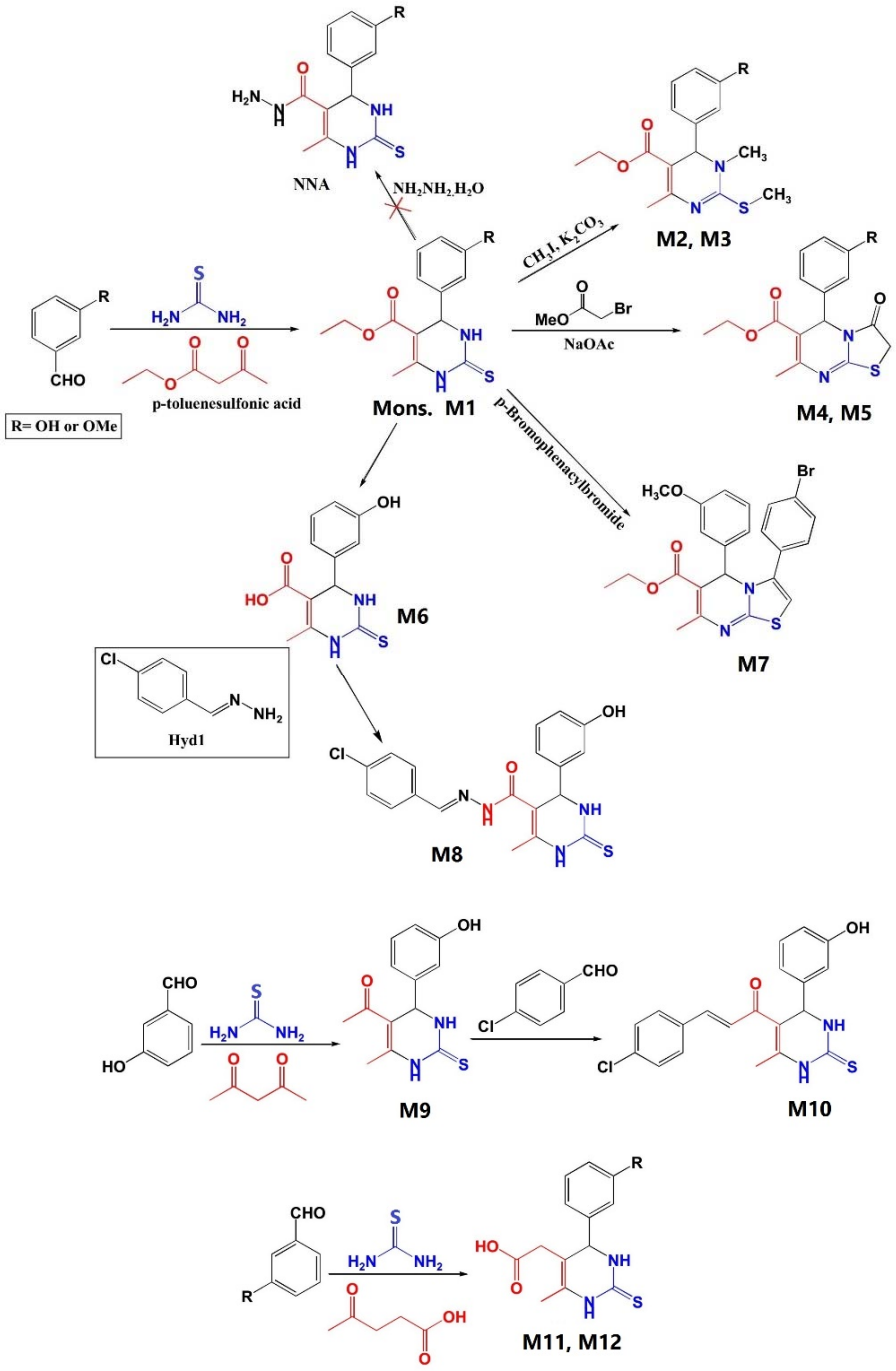

Fig. 1. The overall reaction pathways used to the synthesis of Monastrol's derivatives.

AutoDock Tools were used to generate both grid and docking parameter files. Finally, the free binding energies and inhibition constants (Ki) were calculated. We validated this procedure by the extraction of the monastrol from X-ray complex and redocking it and then superimposing the best-obtained pose with its X-ray counterparts in the 1Q0B structure. The docking poses results were analyzed with AutoDock tools and DS visualizer 3.5.

General chemical procedure for the synthesis of compounds (monastrol-M12)

Synthesis of ethyl 1,2,3,4-tetrahydro-4-(3-hydroxyphenyl)-6-methyl -2- thioxopyrimidine-5-carboxylate) (monastrol) and ethyl 1,2,3,4-tetrahydro-4-(3- methoxyphenyl)- 6-methyl- 2-thioxopyrimidine-5-carboxylate (M1) (4)

A solution of ethyl acetoacetate (60 mmol), aldehyde (40 mmol), and thiourea (60 mmol) in the minimum amount of ethanol (10-15 mL) was prepared. In the presence of the catalytic amount of p-toluenesulfonic acid (PTSA, 6 mmol), the medium was refluxed for 6-8 h. After the completion of the reaction, the mixture was cooled, and 10 mL of cold ethanol was added to it and kept cold overnight. White to yellow precipitates were filtered and rewashed with cold water and ethanol. In the case of monastrol, the product was further purified by recrystallization from ethyl acetate.

Synthesis of ethyl 3,5-dihydro-5-(3-hydroxyphenyl)-7-methyl-3-oxo-2H-thiazolo[3,2-a] pyrimidine-6-carboxylate (M2) and ethyl 3,5-dihydro-5-(3-methoxyphenyl)-7-methyl-3-oxo-2H-thiazolo[3,2-a] pyrimidine-6-carboxylate (M3) (14)

A mixture of compound monastrol or **M1** (2 mmol), methyl bromoacetate (2 mmol), and anhydrous sodium acetate (400 mg) was refluxed in anhydrous ethanol for 5 h. The solvent was evaporated under vacuum, and the product was recrystallized from ethyl acetate.

Synthesis of ethyl 1,6-dihydro-6-(3-hydroxyphenyl)-1,4-dimethyl-2-(methylthio) pyrimidine-5-carboxylate (M4) and ethyl 1,6-dihydro-6-(3-methoxyphenyl)-1,4-dimethyl-2-(methylthio) pyrimidine-5-carboxylate (M5) (15)

To a solution of monastrol or **M1** (2 mmol) in DMF (5 mL), potassium carbonate (4 mmol) and methyl iodide (4 mmol) was added, and the mixture was stirred for 7-10 h in room temperature. After completion of the reaction, the mixture was poured into cold water, and precipitates were recrystallized from ethanol.

Synthesis of 1,2,3,4-tetrahydro-4-(3-hydroxyphenyl) -6 - methyl- 2- thioxopyrimidine-5-carboxylic acid (M6)(16)

A solution of NaOH (4 mmol) in 1 mL water was added to a solution of compound monastrol (2 mmol) in 5 mL methanol. The mixture was heated and stirred at 60 to 62 °C for 8 h. After the completion, the solvent was removed under vacuum. The residue was then added to 25 mL ice-cold water and was extracted with chloroform (3 × 10 mL) to remove the unreacted ester. The aqueous layer was acidified to pH 2 using 10% v/v HCl and extracted with ethyl acetate (3 × 15 mL). The organic layer was separated, dried over anhydrous sodium sulfate, and concentrated to give the crude acid. The crude acid was purified by PTLC.

Synthesis of ethyl 3-(4-bromophenyl)-8, 8a-dihydro-5-(3-methoxyphenyl)-7-methyl-5H-thiazolo[3,2-a]pyrimidine-6-carboxylate (M7) (17)

A mixture of compound **M1** (4 mmoL), p-bromo phenacyl bromide (4 mmoL), and PTSA (10 mol%) in glacial acetic acid stirred in 100 °C for 4 h, followed by fast reflux at 120 °C about 2 h. After completion of the reaction, the vessel was kept overnight at room temperature. The mixture was added into stirring ice-cold water, and the precipitates were filtered, washed with water and petroleum ether to obtain pure product. Upon the neutralizing of the filtrate (NaHCO3 5%), we got the next portion of precipitates, which was purified the same as before.

Synthesis of (17E)-N'-(4-chlorobenzylidene)-1,2,3,4-tetrahydro- 4- (3- hydroxyphenyl)-6-methyl-2-thioxopyrimidine-5-carbohydrazide (M8) (18)

4-Chlorobenzaldehyde (5 g) was added to a stirred mixture of hydrazine hydrate (99% in water, 7 mL) and toluene (10 mL) over 0.5 h at 50 °C. After an additional 1 h at 50 °C, the mixture was cooled to room temperature and diluted with water (5 mL). The organic layer was separated and concentrated to dryness in a vacuum. The residue was slurried in heptane (30 mL) and filtered. The dried yellow powder (Hyd1), brought to reaction with activated acid, immediately. Compound M6 (0.38 mmol) was dissolved in anhydrous DMF (10 mL). To this solution was added EDC, HOBt (both 0.42 mmol), **Hyd1** (0.38 mmol), and the mixture

stirred at room temperature for 4 h. The medium was concentrated under a vacuum. We added ethyl acetate and hexane mixture to the remaining, and the resulting precipitants were purified by PTLC.

Synthesis of 1-(1,2,3,4- tetrahydro -4- (3-methoxyphenyl)-6-methyl-2-thioxopyrimidin-5-yl)ethanone (M9) (19)

A solution of 3-methoxybenzaldehyde (5 mmol), acetylacetone (7.5 mmol), thiourea (6.5 mmol), and two drops of concentrated HCl in absolute ethanol (10 mL) was stirred at 50-55 °C for 20 h. One drop of concentrated HCl was added occasionally. After the completion of the reaction, it was kept at 0 - 4 °C overnight, the precipitate was filtered and recrystallized from ethanol to afford M9 as a yellowish solid.

Synthesis of (2E)-1-(1, 2, 3, 4-tetrahydro-4-(3-methoxyphenyl)-6-methyl-2-thioxopyrimidin-5-yl)-3-(4-chlorophenyl)prop-2-en-1-one (M10) (20)

A mixture of M9 (2 mmol) and the 4-chlorobenzaldehyde (2 mmol) in 10% ethanolic sodium hydroxide solution (5 mL) was stirred at room temperature for 24 h following by 1 h reflux. The mixture was cooled, poured onto ice water (20 mL), and neutralized with 37% HCl (0.5 mL). The precipitates were filtered, dried, and recrystallized from aqueous DMF to give the final product as a yellow powder.

Synthesis of 2-(1,2,3,4-tetrahydro-4-(3-hydroxyphenyl)-6-methyl-2-thioxopyrimidin-5-yl) acetic acid (M11) and 2-(1,2,3,4-tetrahydro-4-(3- methoxyphenyl)-6- methyl- 2-thioxopyrimidin-5-yl) acetic acid (M12)(21)

3-Hydroxy benzaldehyde/ 3-methoxy benzaldehyde (10 mmol), thiourea (10 mmol), and PTSA (1 mmol) were dispersed in 10 mL ethanol, and to this, levulinic acid (10 mmol) was added. The mixture was stirred at 80 °C for 24 h. Ethanol was removed under vacuum, and the remaining sticky product was dissolved in 10 mL water (pH adjusted to 2), and 15 mL ethyl acetate. The organic layer then separated dried over anhydrous sodium sulfate, and removed; the pure product was obtained by recrystallization in glacial acetic acid.

in vitro cytotoxicity assay

The cell lines (MCF-7 and HeLa) were cultured in a complete medium (RPMI 1640 medium supplemented with 10% FBS, 1% antibiotic, penicillin/streptomycin). Stock solutions of compounds with a concentration of 10000 µM were prepared in sterile DMSO. Before treatment, the concentrations of 100, 500, 1000, 1500, 2000, and 3000 µM were prepared using the complete medium. Cells were incubated in 96-well plates containing 170 µL of complete medium per well and at a density of 5000 cells/well. After 24 h incubation at standard conditions and complete cell adhesion, 20 µL of each concentration was added to the assigned wells (the maximum concentration of DMSO in each well was justified at 2%). The final concentrations were 10, 50, 100, 150, 200, and 300 µM. Positive control wells (other than monastrol, and for better monitoring of cell line sensitivity) containing 2 mg/mL paclitaxel (Hangzhou, China), prepared in the same manner, along with negative control and blank wells. After 48 h incubation, the supernatant medium of each well, containing soluble chemicals and dead cells, replaced with 100 µL phenol red-free RPMI. Then MTT solution (10 µL, 5 mg/mL in RPMI) was added, and plates were incubated for 3 h, the medium of each well was carefully eliminated, and 100 µL DMSO was added to each well to remove formazon, and the absorbance was measured using a microplate reader at 570 nm. The cell viability was calculated using the following equation:

$$\text{Cell survival (\%)} = \frac{(Tm - Bm)}{Cm - Bm)} \times 100$$

where Tm, Bm, and Cm represent mean absorbance of the treatment, blank, and negative control, respectively (22). The above assay was repeated in triplicate, and final mean cell survival used to calculate IC50 of each compound using excel software.

Statistical analysis

To compare the statistical differences between groups, one way ANOVA was run in SPSS software, and followed up with post-hoc tests with significant level set at 0.05. Data are presented as mean ± SEM.

RESULTS

Docking studies

The results of this part, including the values for free binding energy (ΔG_{bind}) and other details for the best-docked positions in the active site of Eg5, are provided in Tables 1 and 2. The molecular interactions of the best redocked pose of monastrol, as well as the best-docked poses of **M4** and **M11** within the active site, are depicted in Fig. 2.

Chemistry

All of the chemical reactions are shown in Fig. 1, and the proposed mechanism of ring cleavage in the reaction with hydrazine is provided in Fig. 3.

Furthermore, all of spectral details for various derivatives are as follow:

monastrol: Yield: 65%; pale yellow powder; melting point (MP): 185-187 °C (lit. 185-186 °C (24)); $C_{14}H_{16}N_2O_3S$; IR ν_{max} cm^{-1}: 3308 (broad band; O-H and N-H str.), 3184 (C-H str. aromatic), 2981 (C-H str. aliphatic), 1667 (C=O str.), 1574 (Ar. C=C str.), 1471 (C-H bend.), 1279 (C-N str.), 1191 (C=S str.); ^{1}HNMR (DMSO-d6) δ ppm: 10.39 (s, 1H, N-H), 9.69 (d, 1H, N-H, J = 2.80 Hz), 9.53 (s, 1H, O-H), 7.19 (m, 1H, H Ar.), 6.70-6.73 (m, 3H, H Ar.),5.17 (d, 1H, J = 2.80 Hz), 4.09 (m, 2H, -OCH2CH3), 2.35 (s, 3H, Ar-CH3), 1.20 (t, 3H, -OCH2CH3).

M1: Yield: 78%; pale yellow powder; MP: 167-168 °C; $C_{15}H_{18}N_2O_3S$; IR ν_{max} cm^{-1}: 3298 (broad band; O-H and N-H str.), 3180, 3102, 2906, 1661 (C=O str.), 1595 (N-H bend.), 1571 (C=C aromatic), 1459, 1254, 1189 (C=S str.); ^{1}HNMR (DMSO-d6) δ ppm: 10.35 (s, 1H, N-H), 9.65 (d, 1H, N-H, J= 2.4 Hz), 7.26-7.30 (m, 1H, H Ar.), 6.76-6.88 (m, 3H, H Ar.), 5.16 (d, 1H, H4, J = 2.4 Hz), 4.01-4.06 (m, 2H, -OCH2CH3), 2.29 (s, 3H, Ar-CH3), 1.13 (t, 3H, -OCH2CH3, J = 6.8 Hz).

M2: Yield: 78%; white powder; MP: 210-212 °C (lit. 219 °C(25)); $C_{16}H_{16}N_2O_4S$; IR ν_{max} cm^{-1}: 3413 (O-H str.), 2984 (C-H str. aliphatic), 1742 (C=O str.), 1696 (C=O str.), 1541, 1236 (C-N str.), 1173 (C=S str.); ^{1}HNMR ($CDCl_3$) δ ppm: 9.52 (s, 1H, O-H), 7.09-7.14 (m, 1H, H Ar.), 6.71-6.90 (m, 3H, H Ar.), 5.96 (s, 1H, H4), 4.04-4.92 (m, 2H, -OCH2CH3), 3.69-3.99 (dd, 2H, J = 17.2 Hz), 2.39 (s, 3H, Ar-CH3), 1.12 (t, 3H, -OCH2CH3).

M3: Yield: 60%; pale yellow crystals; MP: 118-119 °C; $C_{17}H_{18}N_2O_4S$; IR ν_{max} cm^{-1}: 3060 (C-H str. aromatic), 2992 (C-H str. aliphatic), 2965, 1735 (C=O str.), 1700 (C=O str.), 1603 (N-H bend.), 1536, 1381, 1227, 1167 (C-S str.); ^{1}HNMR (CDCl3) δ ppm: 7.15 (m, 1H, H Ar.), 6.62-6.77 (m, 3H, H Ar.), 5.85 (s, 1H, H4), 4.05 (m, 2H, -OCH2CH3), 3.70-3.83 (dd, 2H, J = 14 Hz), 3.60 (s, 3H, -OCH3), 2.20 (s, 3H, Ar-CH3), 1.01 (t, 3H, -OCH2CH3).

Table 1. Docking results of the proposed compounds and reference ligand (monastrol) into the Eg5 active site (pdb code: 1Q0B).

Derivatives	ΔG_{bind} (kcal/mol)	VHDE (kcal/mol)	EE (kcal/mol)	IE (kcal/mol)	IC (μM)
M1	-6.34	-7.81	-0.01	-7.83	22.67
M2	-6.09	-6.86	-0.13	-6.99	34.18
M3	-5.67	-7.06	0.19	-6.87	69.55
M4	-8.01	-9.79	0.00	-9.8	1.35
M5	-6.24	-7.48	0.05	-7.43	26.76
M6	-7.16	-8.47	-0.18	-8.65	5.63
M6-1	-6.90	-8.34	-0.06	-8.40	8.70
M7	-3.05	-4.70	-0.14	-4.84	5810
M8	-6.51	-7.21	-0.2	-7.41	16.8
M9	-7.29	8.68	-0.4	-9.08	4.57
M10	-5.53	-6.66	0.24	-6.43	88.22
M11	-8.63	-10.10	-0.02	-10.12	0.473
M12	-6.54	-8.34	0.00	-8.33	16.01
Monastrol (Cocrystalized ligand)	-6.67	-8.06	-0.1	-8.16	12.95

VHDE, Vander Waals H-bond desolvatio energy; EE, electrostatic energy; IE, intermolecular energy; IC, inhibitory concentration.

Table 2. Details of interaction between the docked compounds and the Eg5 binding site residues (pdb code: 1Q0B).

Derivatives	Amino acids in hydrophobic interaction	Amino acids in hydrogen bond interaction	Amino acids in cation-π interaction	Amino acids in electrostatic interaction
M1	Arg119, Trp127, Ile136, Pro137, Leu160, Tyr211, Leu214, Phe239	Gly117, Glu116	-	Arg221, Glu118, Glu116
M2	Thr112, Arg119, Ala133, Ile136, Pro137, Leu160, Tyr211, Leu214, Ala218, Phe239	Gly117	Arg221	Arg221, Glu116,
M3	Arg119, Ile136, Leu160, Tyr211, Leu214, Ala218, Phe239	Arg221	-	Arg221, Glu116,
M4	Thr112, Glu118, Arg119, Ile136, Tyr211, Ala133, Trp127, Pro137, Ile136, Leu160, Leu214, Ala218	Glu116	Arg221	Arg221, Glu116
M5	Arg119, Trp127, Ile136, Pro137, Leu160, Tyr211, Leu214, Phe239	-	-	Arg221, Glu118, Glu116
M6	Met115, Leu132, Ala133, Ile136, Pro137, Tyr211, Leu214, Ala218	Glu118	Arg119	Glu116, Arg119, Glu118
M6-1	Ile136, Pro137, Leu160, Tyr211, Leu214, Ala218	Glu116	Arg221	Arg119, Glu116, Arg221
M7	Gly117, Ile136, Leu214, Ala218, Pro136	Arg221	-	-
M8	Arg119, Ala133, Ile136, Pro137, Tyr211, Leu214	Leu214, Gly117	-	Glu118, Glu116, Arg221
M9	Leu132, Ala133, Ile136, Pro137, Tyr211, Leu214, Ala218	-	-	Glu118, Glu116, Arg119
M10	Ala133, Ile136, Pro137, Tyr211, Leu214, Ala218	Glu116	-	Glu118, Glu116, Arg119, Arg221
M11	Ser120, Trp127, Leu132, Ala133, Gly134, Ile136, Pro137, Tyr211, Ala218, Asp130	Glu118, Gly117	Arg119	Glu118, Glu116, Arg119
M12	Thr112, Ile136, Pro137, Leu160, Tyr211, Leu214, Ala218	Glu116	Arg221	Glu116, Arg119, Arg221
Monastrol (cocrystalized ligand)	Gly117, Ser120, Trp127, Asp130, Leu132, Ala133, Gly134, Ile136, Pro137, Tyr211, Leu214, Glu215, Ala218	Glu118, Glu116	Arg119	Glu118, Glu116, Arg119

M4: Yield: 80%; white fine powder; MP: 153-155 °C (lit. 150-152 °C (26)); $C_{16}H_{20}N_2O_3S$; IR ν_{max} cm^{-1}: 3312 (O-H str.), 2932 (C-H str. aliphatic), 1654 (C=O str.), 1590 (N-H bend.), 1479, 1275 (C-N str.), 1182 (C=S str.); ^{1}HNMR (DMSO-d6) δ ppm: 9.55 (s, 1H, O-H), 7.29-7.33 (m, 1H, H Ar.), 6.82-6.84 (m, 3H, H Ar.), 5.41 (s, 1H, H4), 4.10-4.15 (m , 2H, -OCH2CH3), 3.11 (s, 3H, -N-CH3), 2.66 (s, 3H, -S-CH3), 2.35 (s, 3H, Ar-CH3), 1.19 (t, 3H, -OCH2CH3).

M5: Yield: 70%; yellow crystals; MP: 161-162 °C; $C_{17}H_{22}N_2O_3S$; IR ν_{max} cm^{-1}: 3046 (C-H str. aromatic), 2985, 1664 (C=O str.), 1597 (N-H bend.), 1507 (C=C Ar.), 1369 (C-O str.), 1248 (C=S str.); ^{1}HNMR (DMSO-d6) δ ppm: 7.36-7.40 (m, 1H, H Ar.), 6.90-6.98 (s, 3H, H Ar.), 5.36 (s, 1H, H4), 4.06-4.15 (m, 2H, -OCH2CH3), 3.83 (s, 3H, -OCH3), 3.08 (s, 3H, -N-CH3), 2.37 (s, 3H, Ar-CH3), 1.24 (t, 3H, -OCH2CH3).

M6: Yield: 20%; white powder; MP: 168-170 °C (lit. 163-165 °C(16)); $C_{12}H_{12}N_2O_3S$; IR ν_{max} cm^{-1}: 3381 (O-H str.), 3270 (N-H str.), 3172 (N-H str.), 3095, 1610 (C=O, acid), 1470, 1413, 1185 (C=S str.); ^{1}HNMR (DMSO-d6) δ ppm: 12.15 (bs, 1H, COOH), 10.39 (s, 1H, N-H), 9.69 (d, 1H, N-H, J = 1.20 Hz), 7.23-7.27 (m, 1H, H Ar.), 6.72-6.89 (m, 3H, H Ar.), 5.19 (d, 1H, H4, J = 1.2 Hz), 3.71 (s, 3H, -OCH3), 2.27 (s, 3H, Ar-CH3).

M7: Yield: 48%; yellow-brown powder; MP: 228-229 °C; $C_{23}H_{23}BrN_2O_3S$; IR ν_{max} cm^{-1}: 3107 (N-H str.), 2959, 1706 (C=O str.), 1650 (C=O str.), 1583 (Ar. C=C), 1530, 1484, 1260 (C=S str.); ^{1}HNMR (DMSO-d6) δ ppm: 7.82 (d, 2H, H Ar.), 7.56 (s, 1H, H Ar.), 7.36 (d, 2H, H Ar., J = 8.4 Hz), 7.19-7.23 (m 1H, H Ar.), 6.87-6.89 (m, 1H, H Ar.), 6.49-6.51 (m, 1H, H Ar.), 6.36 (s, 1H, H Ar.), 6.11 (s, 1H, H4), 4.07-4.20 (m, 2H, -OCH2CH3), 3.63 (s, 3H, -OCH3), 2.54 (s, 3H, Ar-CH3), 1.18 (t, 3H, -OCH2CH3);

^{13}CNMR (100 MHz, DMSO-d6, δ (ppm): 164.43, 161.24, 159.26, 141.05, 139.27, 132.29, 132.19, 130.57, 127.07, 124.82, 119.30, 115.01, 112.82, 112.30, 103.22, 70.24, 61.02, 59.41, 55.28, 18.43, 14.36.

Hyd1: Yield: 75%; yellow crystal; MP: 65-66 °C; $C_7H_7ClN_2$; ^{1}HNMR ($CDCl_3$) δ ppm: 8.54 (s, 1H, -CH=N-), 7.72 (d, 2H, H Ar., J= 8.40 Hz), 7.36 (d, 2H, H Ar., J = 8.40 Hz), 2.11 (s, 2H, NH2).

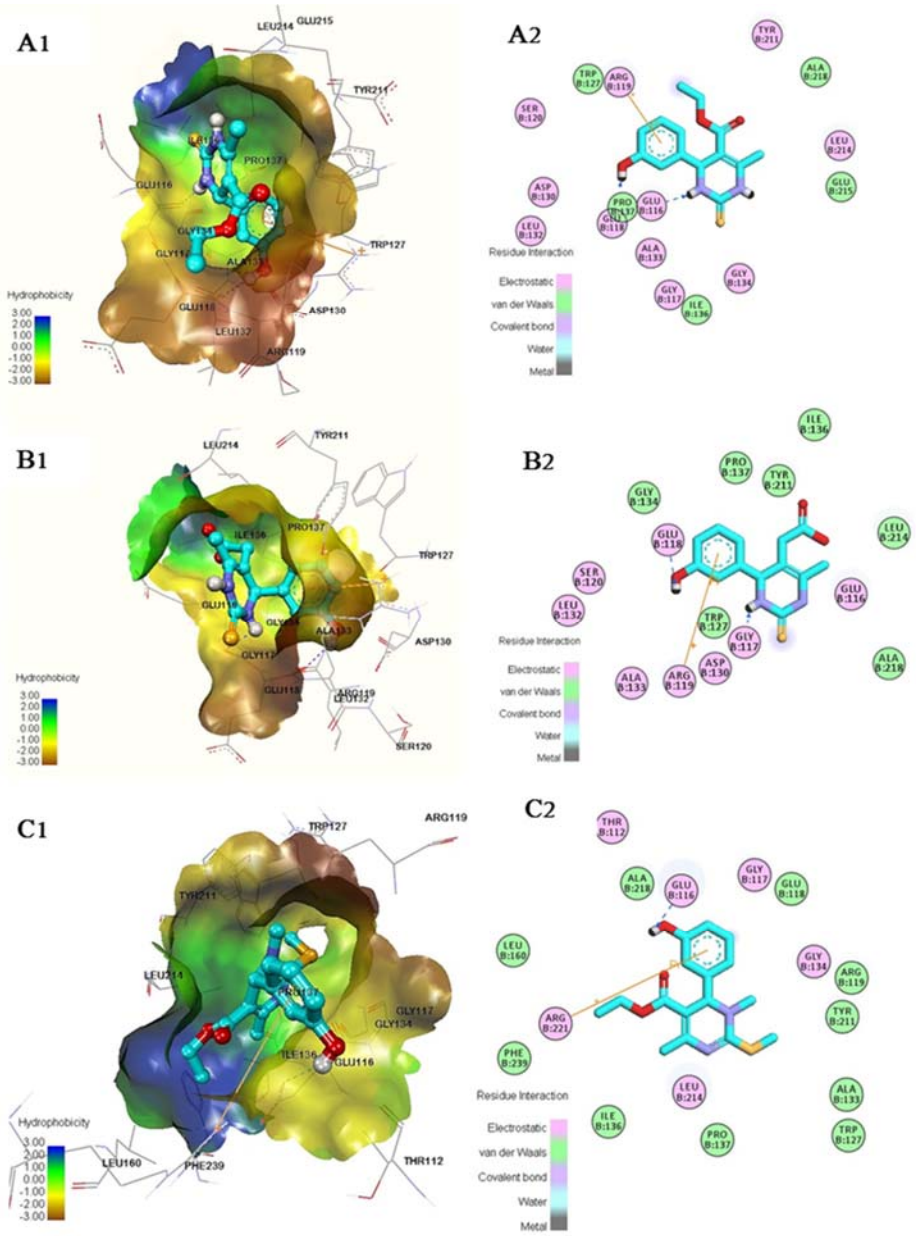

Fig. 2. (A_1-C_1) Best redocked pose of the monastrol, **M11,** and **M4** in the Eg5 active site; (A_2-C_2) two dimensional diagram of the interaction between the redocked monastrol, **M11**, and **M4** and the critical interacting amino acid residues of binding site. Blue dashed line shows hydrogen bonds and π cationic interaction is represented as an orange line. Figures are prepared using the Accelrys discovery studio visualizer program.

M8: Yield: 13%; yellow powder; MP: 126-128 °C; $C_{19}H_{17}ClN_4O_2S$; IR ν_{max} cm^{-1}: 3383 (broad band; O-H and N-H str.), 3186, 2963, 1657 (C=O str.), 1592 (C=C str. and N-H bend.), 1482, 1262 (C-N str.), 1189 (C=S str.); ^{1}HNMR (DMSO-d6) δ ppm: ^{13}CNMR (100 MHz, DMSO-d6, δ (ppm): 10.38 (s, 1H, N-H), 9.69 (s, 1H, N-H, J= 2.40), 9.53 (s, 1H, O-H), 8.22 (s, 1H, -C=N-NH-CO-), 7.83 (s, 1H, -CH=N-), 7.63 (d, 2H, H Ar., J = 8.40 Hz), 7.51 (d, 2H, H Ar., J = 8.40 Hz), 7.19 (m, 1H, H Ar.), 6.71-6.73 (m, 3H, H Ar.), 5.15 (d, 1H, H4, J = 2.80 Hz), 2.35 (s, 3H, Ar-CH3); ^{13}CNMR (100 MHz, DMSO-d6, δ (ppm): 178.1, 169.1, 158.2, 150.1, 143.3, 142.1, 130.5, 130.0, 129.4, 129.0, 117.4, 115.1, 113.8, 109.5, 52.9, 16.9.

M9: Yield: 85%; yellow powder; MP: 252-254 °C; $C_{14}H_{16}N_2O_2S$; IR ν_{max} cm^{-1}: 3402 (N-H str.), 3301 (O-H str.), 2981 (C-H str. aliphatic), 1660 (C=O, str.), 1590 (N-H, bending), 1505 (C=C), 1432 (C-C), 1373 (C-N), 1181 (C=S str.); ^{1}HNMR (DMSO-d6) δ ppm: 10.26 (s, 1H, N-H), 9.72 (d, 1H, N-H, J = 2.40 Hz), 7.11-7.15 (m, 1H, H Ar.), 6.65-6.68 (m, 3H, H Ar.), 5.20 (d, 1H, H4, J = 2.40 Hz), 3.84 (s, 3H, -OCH3), 2.32 (s, 3H, Ar-CH3), 2.14 (s, 3H, CH3-CO-).

M10: Yield; 70%; yellow powder; MP:171-173 °C; $C_{21}H_{19}ClN_2O_2S$; IR ν_{max} cm^{-1}: 3328, 3320 (N-H str.), 3026, 2935, 1690 (C=O str.), 1621 (C=C str.), 1561 (C=C str.), 1185 (C=S str.); ^{1}HNMR (DMSO-d6), δ (ppm): 10.04 (s, 1H, N-H), 9.20 (d, 1H, N-H, J = 1.20 Hz), 7.68 (d, 2H, H Ar., J = 7.60 Hz), 7.38 (m, 1H, H Ar.), 7.17 (d, 2H, H Ar., J = 7.60 Hz), 6.89-6.99 (m, 3H, H Ar.), 6.18 (d, 1H, -CH=CH-CO-, J = 11.20 Hz), 5.37 (d, 1 H, H4, J = 1.20 Hz), 3.83 (s, 3H, -OCH3), 2.37 (s, 3H, Ar-CH3).

M11: Yield: 27%; off white powder; decomposition point around 200 °C; $C_{13}H_{14}N_2O_3S$; IR ν_{max} cm^{-1}: 3279 (broad bands of O-H and N-H str.), 2985, 1700 (C=O str.), 1679 (C=O str.), 1599 (N-H bend.), 1479, 1455, 1229 (C-S str.); ^{1}HNMR (DMSO-d6) δ ppm: 12.10 (bs, 1H, COOH), 10.25 (s, 1H, N-H), 9.69 (d, 1H, N-H, J =2.80 Hz), 7.07-7.11 (m, 1H, H Ar.), 6.77-6.79 (m, 3H, H Ar.), 5.19 (d, 1H, H4, J = 2.80 Hz), 2.85 (s, 2H, -CH2-CO-), 2.35 (s, 3H, Ar-CH3).

M12: Yield: 28%; pale yellow powder; MP: 127-129 °C; $C_{14}H_{16}N_2O_3S$; IR ν_{max} cm^{-1}: 3408 (N-H str.), 3278, 2912, 1715 (C=O str.), 1617 (C=C), 1474, 1425, 1223 (C-S str.); ^{1}HNMR (DMSO-d6) δ ppm: 12.15 (bs, 1H, COOH), 10.35 (s, 1H, N-H), 9.65 (d, 1H, N-H, J =2.80 Hz), 7.26-7.30 (m, 1H, H Ar.), 6.77-6.87 (m, 3H, H Ar.), 5.15 (d, 1H, H4, J = 2.80 Hz), 3.74 (s, 3H, -OCH3), 2.71 (s, 2H, -OCH2CH3), 2.30 (s, 3H, Ar-CH3); ^{13}CNMR (100 MHz, DMSO-d6, δ (ppm):178.3, 171.9, 160.1, 142.5, 136.3, 130.4, 121.5, 116.9, 113.5, 106.6, 82.2, 55.7, 35.4, 28.2.

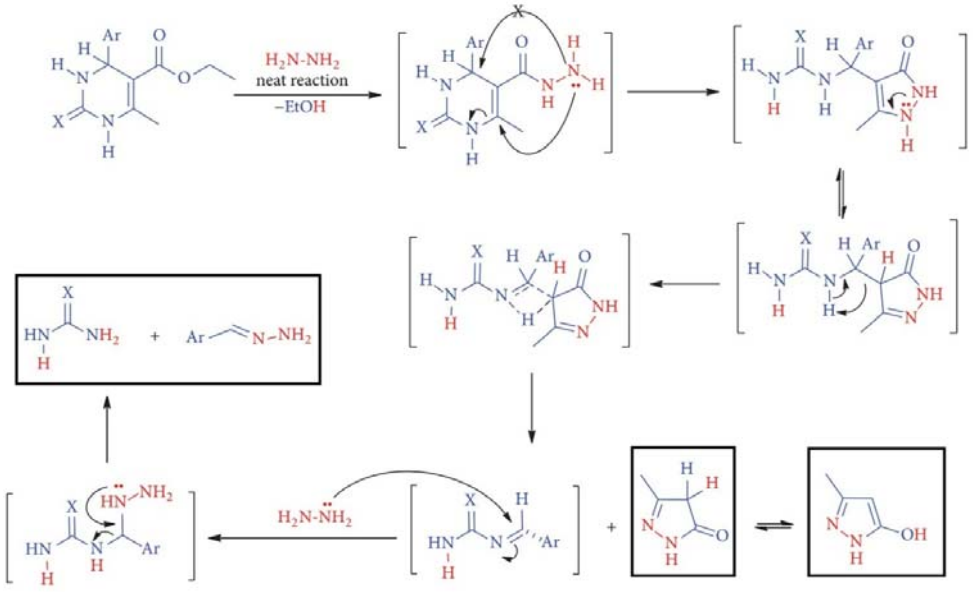

Fig. 3. Proposed decomposition mechanism of dihydropyrimidinone by hydrazinolysis, reported by Said *et al.* (23).

Evaluation of cytotoxic effect

All of the estimated IC_{50} values on MCF-7 and Hela cells are provided in Table 3.

Table 3. Evaluated IC_{50} values of monastrol's derivatives for MCF-7 and HeLa cell lines and the $\Delta G_{bind.}$ The IC_{50} valus are presented as mean ± SEM.

Derivatives	IC_{50} values		ΔG bind (kcal/mol)
	MCF-7	HeLa	
Monastrol	88 ± 23	111 ± 25	-6.67
M1	138 ± 6	160 ± 6	-6.34
M2	175 ± 20	224 ± 20	-6.09
M3	145 ± 3	232 ± 3	-5.67
M4	164 ± 21	220 ± 21	-8.01
M5	183 ± 22	262 ± 22	-6.24
M6	171 ± 15	217 ± 15	-7.16
D_2	Not evaluated	Not evaluated	-6.90
M7	167 ± 1	270 ± 1	-3.05
M8	187 ± 5	225 ± 5	-6.51
M9	168 ± 15	228 ± 15	-7.29
M10	230 ± 63	249 ± 63	-5.53
M11	194 ± 30	266 ± 30	-8.63
M12	205 ± 13	> 500	-6.54

DISCUSSION

In order to better rationalize SAR of the proposed monastrol's analogs and gain insights into the binding mode of molecules within the motor domain of Eg5, molecular docking studies were conducted. Among available X-ray structures of the Eg5-monastrol complex, the structure (PDB ID: 1Q0B) with a high resolution (1.9 Å) was chosen (6, 27-29). The accuracy of the docking protocol was validated by removing the co-crystallized monastrol from the binding site of Eg5 and redocking into the active site. The results of the redocking indicated that the redocked conformer of monastrol adopted a similar binding mode to that seen in its parent crystal structure. The root mean square deviation (RMSD) value for this compound in comparison with its coordination in the crystal structure was 0.14. Based on Fig. 1A, the redocked monastrol have favorable hydrophobic with a relatively hydrophobic region within the active site surrounded by Trp127, Leu132, Ala133, Ile136, Pro137, Tyr211, Leu214, Glu215, Ala218 amino acid residues. The ligand-binding was further stabilized by favorable hydrogen bonds with crucial residues same as the original cocrystal monastrol. Moreover, for redocking analysis, with the same orientation as we see in the cocrystal structure, the 4-phenyl group was involved in a cation-π interaction with the residue of Arg119. According to these results, the moderate degree of hydrophobicity and the ability to establish hydrogen bonds with Glu118 and Glu116, can be considered as the prime determinants for the binding affinity of inhibitors to the active site. After the validation, as it can be seen from Table 1, all of the proposed derivatives were docked into the same binding site of the Eg5 with negative binding energy values**.** Previous studies using hydrogen-deuterium exchange and mass spectrometry coupled with directed mutagenesis on the motor domain of human Eg5 pointed out the importance of these interactions at monastrol's binding site (30). As Table 1 shows, the *in-silico* inhibition trend of proposed derivatives was as following; M11 > M4 > M9 > M6 > D2 > monastrol >M12 > M8 > M1 > M5> M2 > M3 > M10 > M7.

Among all of derivatives, compounds M4 and M11 were particularly found to possess better binding affinity (ΔG_{bind}: -8.63 and -8.01 Kcal/mol, respectively) than monastrol (ΔG_{bind}: -6.67 Kcal/mol). The best-docked pose of M11 within the active site is depicted in Fig. 1B. As this figure shows, the compound displayed the same pattern of hydrogen bonding interaction with Glu118 as observed for monastrol (Fig. 1A). Moreover, the phenyl ring of the C4 position is situated in such a way that favorably made a π–cationic interaction with a positively charged amino group of the Arg119. Based on the previous reports, hydrophobic and electrostatic interactions of the ligand with Arg119 appear to be crucial for drug binding at the motor domain of human Eg5, therefore the Eg5 motor domain is remarkably tolerant of mutations at Arg119 (31). A comparison of the docking energy values of M11 (ΔG_{bind}: -8.63 Kcal/mol) and M6 (ΔG_{bind}:-7.16 Kcal/mol) indicated that the insertion of an additional methylene unit to the junction of the C5 and carboxylic acid side chain was in favor of binding affinity to the Eg5 active site. This result could be due to the increased flexibility of the C-5 carboxylic acid side chain that enables it to deeper access toward the

hydrophilic residues. For **M11**, more effective hydrophobic interactions may be achieved with Gly134, Pro137, Ile136, Tyr211, and Leu214 residues. Based on this analysis, the free binding energy can also be improved through N3 and S methylation. In this regard, the N/S-methylated analogs of monastrol, **M4**, displayed more affinity to interact with the active site (ΔG_{bind}: -8.01 Kcal/mol). Despite the participation of this compound in the only one hydrogen binding with Glu116, the more hydrophobic interactions of N/S-methyl fragments with the non-polar residues, especially Tyr211, Ala133, Trp127, and Pro137 could promote the affinity (Fig. 1C). Interestingly, the docking models revealed that the replacement of hydroxyl substituent at the meta position of the phenyl ring in **M11** by a methoxy group in compound **M12** led to a reduction in the binding affinity (ΔG_{bind}: -6.54 Kcal/mol). Compound **M12** adopted a conformation in which the 3-methoxy substituted phenyl ring was pointed to the opposite direction as that seen in **M11**. Although in this orientation phenyl ring participated in a π cationic interaction with Arg221, no meaningful hydrogen bonding could be detected between the methoxy group and critical residues. Similar findings were obtained for **M5** (ΔG_{bind}:-6.24 Kcal/mol) comparing the corresponding 3-hydroxy substituted analog **M4** (ΔG_{bind}: -8.01 Kcal/mol), **M5** did not make any vital hydrogen bonding and π cationic interactions. As shown in Table 1, **M2**, **M3**, and **M10** exhibited significantly more reduced affinities compared to monastrol. The ΔG_{bind} values of the best docked poses of these compounds were within the range of -6.09 to -5.53 Kcal/mol. Further bulky substitutions at the positions of C_2, N_3, and C_5 of the primary scaffold could hamper the binding affinity to the active site. Limited extension of binding pocket can be attributed to the more accessible accommodation and so better fitting of small groups at the active site compared with bulkier ones. The importance of this issue is more noticeable about bicyclic compound **M7**. Because of bulky 4-bromophenyl moiety, **M7** was not able to entirely insert in the binding pocket ΔG_{bind}: -3.05 Kcal/mol). Generally, docking results of proposed compounds were in a satisfactory agreement with the published cocrystal structure of monastrol with the Eg5 motor domain (32)as well as the SAR reported for different kinds of monastrol's derivatives by other research groups (6,29,30).

The synthesis pathways for all derivatives are shown in Fig. 2. Monastrol and **M1** were synthesized without any complications, as described in the literature, using PTSA and anhydrous sodium acetate as the primary catalysts, respectively (4,14). We synthesized dimethyl monastrol at S, and N3 (rather than the N1) positions using methyl iodide and potassium carbonate with a slight modification to an earlier report (15). In the next step, the reaction between monastrol and hydrazine hydrate did not proceed, as mentioned in the literature (33), and we could not obtain any pure carboxyhydrazide (compound **X**). Other efforts with different conditions were studied instead, but we could not succeed in any of them to the synthesis of **X**. The product of all these attempts was the initial monastrol (confirmed by HNMR) or different products that could not be separated as pure compounds. It seems that in mild conditions (equimolar ratios, and low temperature), hydrazine hydrate is not strong enough to lyse the ester group. Whereas in harsh conditions (excess hydrazine hydrate and high temperature), we see the ring decomposition (Fig. 3), as *Said et al.* observed (23) before. Finally, to make a change in the ring position of 5, we tried to get the carboxylic acid forms of our parent ester. The low efficacy of hydrolysis reaction was the main drawback in this pathway. The leading causes are the α,β-unsaturated nature of monastrol ring (34), and wide ranges of pKa present in the acid product (predicted values are 9.38, 11.16, and 3.47 for phenolic hydroxyl, N1, and carboxyl group, respectively). Finally, we purified the **M6** in low yield and obtained **M8** after the reaction of **M6** with **Hyd1**, similar as the reported method (26). Because of the instability of hydrazones, the coupling reaction performed almost *in situ* in the presence of EDC/HOBt as catalysts (18). We synthesized other derivatives (**M2**, **M3**, and **M7**) without any considerable difficulty. In a direct route for the synthesis of **M11** and **M12**, we used levulinic acid as the starting material

instead of ethyl acetoacetate. We preferred PTSA catalyst instead of potassium carbonate as reported before (21), to prevent alkaline mediated decarboxylation of the final product. Finally, we synthesized the acetyl derivative of methoxylated monastrol (**M9**) and chalcone derivative (**M10**) as the complementary derivatives based on the previous reports (19,20) with minor changes. Among the all synthesized derivatives **M5**, **M7**, **M8**, **M11**, **M12**, and **M10** are all novel, and their synthesis is reported for the first time. The spectral proofs confirmed the correct structures. All compounds had their special characteristic features in both NMR and IR spectra. All of the dimethylated derivatives (**M4** and **M5**) are **N3** methylated, which can be approved by the doublet signal for H4 on the ring. Both **M2** and **M3** derivatives showed a specific pattern due to the sulfur's effect on the methylene group of the thiazole ring. For **M8** and **M10**, we have a specific pattern of para substituted phenyl group beside the vinylic proton, which can be seen readily in their NMR spectra.

MCF-7 and HeLa cancer cell lines both have assigned for their overexpression of the Eg5 enzyme (35); therefore, we used these two cell lines to study the cell toxicity of the synthesized compounds. Based on estimated IC_{50} values (Table 2) obtained from MTT assay, monastrol showed more potency than its derivatives (88 and 111 µM for MCF-7 and HeLa, respectively). Furthermore, after monastrol, **M1** with a methoxy group instead of hydroxyl, **M3** with thiazole moiety at C2-N3 position, and the dimethylated monastrol, respectively have lower IC_{50} than others on MCF-7 cell line (Table 2). Guido *et al*. have reported the same results for various substituted monastrol; in their study, just the derivative of 2-hydroxyl phenyl had better activity than the monastrol (9). Furthermore, Table 2 shows a relatively similar trend on HeLa cell line; again, monastrol itself has a better potency; after that, the **M1**, **M6**, **M4**, and **M2**, respectively are at the top of the list. Among our novel synthesized derivatives, it seems that **M11** can be a potential candidate for further cellular assessments on MCF-7, and **M8** has the same condition on the HeLa cell line. Amongst the derivatives with a hydrophobic ligand at thiourea residue, the dimethylated derivative is more potent than the thiazole ones in both cell lines. Another finding from our introductory study was obtained from the HeLa cell line assessment, all of the derivatives even the monastrol itself showed significantly less activity on HeLa cell line compares to the MCF-7. Based on the protein atlas website (www.proteinatlas.org), the expression of Eg5 in terms of TPM (transcripts per million) in the MCF-7 cell line is about 32.5, and in HeLa is 29.8, respectively. Therefore, the lower sensitivity of the HeLa cells may be attributed to the lower expression of the Eg5 enzyme, which should be approved by enzymatic assessment, or to the cell resistance resulting from successive sub-culturing or passaging, which should be checked on the newer source of cells. Furthermore, the study conducted by Tcherniuk *et al*. demonstrated that mutations in the induced-fit binding pocket of Eg5 could confer drug resistance in cells to inhibitors that are known to bind to this pocket, such as monastrol (31).

CONCLUSION

Eg5 has been a favorite target in anticancer drug designing to extend more potent anticancer agents. Our *in-silico* studies revealed that all of the proposed derivatives other than the M7 could be suitable candidates for Eg5 inhibition. SAR analysis and molecular modeling studies revealed that the positioning of a hydrogen bond donor/acceptor on the phenyl ring of the monastrol and hydrophobic group on the thiourea moiety play a critical effect in the inhibition of Eg5 enzyme. We synthesized 13 derivatives with different substitution patterns around the monastrol ring. *In vitro* studies potency results were not in line with those of *in silico* experiments. The IC_{50}s were in the range of 88 to more than 500 µg/mL against HeLa and MCF-7 cell lines. Although the designed compounds were found to have moderate activity against cancer cell lines compared to the monastrol, the results are expected to contribute toward more profound insight into the SAR. The results could be helpful in further monastrol-based drug discoveries. The reason behind the controversy between the *in vitro* and *in silico* results might be that the applied cell-based assays are not appropriate representative of the inhibition of

Eg5 protein. Furthermore, the lower *in vitro* activity of studied derivatives could be due to the suboptimal physicochemical properties that should further be modified *via* structural optimization of these compounds in the future. Finally, we should note that in drug development, some parameters, rather than potency, play an essential role, for example, the normal cell cytotoxicity and so on. Furthermore, we found out that some previous reports and claims on the functionalization of the monastrol ring are not reliable and accurate.

ACKNOWLEDGMENTS

This study was financially supported by the Vice Chancellery of Research of Isfahan University of Medical Sciences, Isfahan, I.R. Iran under the Grant No. 195063.

CONFLICT OF INTEREST STATEMENT

The authors declare no conflicts of interest for this study.

AUTHORS' CONTRIBUTION

The idea was developed by M. Rostami. H. Sirous and M. Rostami designED the molecular docking study. M. Rostami, Gh. Khodarahmi, and F. Hassanzadeh supervised this work. The literature review was done by Z. Bidram, A. Ali Hariri, H. Sirous, and M. Rostami. Data collection and analysis was performed by Z. Bidram, H. Sirous, A.A. Hariri, N. Dana, and M. Rostami. Z. Bidram, M. Rostami, and H. Sirous contributed in manuscript preparation and revision.

REFERENCES

1. Tayebee R, Amini MM, Ghadamgahi M, Armaghan M. $H_5PW_{10}V_2O_{40}$/Pip-SBA-15: a novel reusable organic-inorganic hybrid material as potent Lewis acid catalyst for one-pot solvent-free synthesis of 3,4-dihydropyrimidinones. J Mol Catal A: Chem. 2013;366:266-274. DOI: 10.1016/j.molcata.2012.10.004.
2. Razzaghi-Asl N, Kamrani-Moghadam M, Farhangi B, Vahabpour R, Zabihollahi R, Sepehri S. Design, synthesis and evaluation of cytotoxic, antimicrobial, and anti-HIV-1 activities of new 1,2,3,4-tetrahydropyrimidine derivatives. Res Pharm Sci. 2019;14(2):155-166. DOI: 10.4103/1735-5362.253363.
3. Matos LHS, Masson FT, Simeoni LA, Homem-de-Mello M. Biological activity of dihydropyrimidinone (DHPM) derivatives: a systematic review. Eur J Med Chem. 2018;143:1779-1789. DOI: 10.1016/j.ejmech.2017.10.073.
4. Jin T, Zhang S, Li T. *p*-Toluenesulfonic acid-catalyzed efficient synthesis of dihydropyrimidines: improved high yielding protocol for the Biginelli reaction. Synt Communs. 2002;32(12):1847-1851. DOI: 10.1081/SCC-120004068.
5. Marques LA, Semprebon SC, Niwa AM, D'Epiro GFR, Sartori D, de Fátima Â, *et al*. Antiproliferative activity of monastrol in human adenocarcinoma (MCF-7) and non-tumor (HB4a) breast cells. Naunyn-Schmiedebergs Arch Pharmacol. 2016;389(12):1279-1288. DOI: 10.1007/s00210-016-1292-9.
6. Tawfik HO, El-Moselhy TF, El-Din NS, El-Hamamsy MH. Design, synthesis, and bioactivity of dihydropyrimidine derivatives as kinesin spindle protein inhibitors. Bioorg Med Chem. 2019;27(23):115126. DOI: 10.1016/j.bmc.2019.115126.
7. Russowsky D, Canto RFS, Sanches SAA, D'Oca MGM, de Fátima Â, Pilli RA, *et al*. Synthesis and differential antiproliferative activity of Biginelli compounds against cancer cell lines: monastrol, oxo-monastrol and oxygenated analogues. Bioorg Chem. 2006;34(4):173-182. DOI: 10.1016/j.bioorg.2006.04.003.
8. Reddy S, Suryanarayana CV, Sharmila N, GV Ramana, Anuradha V, Hari Babu B. Synthesis and cytotoxic evaluation for some new dihydropyrimidinone derivatives for anticancer activity. Lett Drug Des Discov. 2013;10(8):699-705. DOI: 10.2174/15701808113109990007.
9. Guido BC, Ramos LM, Nolasco DO, Nobrega CC, Andrade BY, Pic-Taylor A, *et al*. Impact of kinesin Eg5 inhibition by 3,4-dihydropyrimidin-2(1H)-one derivatives on various breast cancer cell features. BMC Cancer. 2015;15:283-297. DOI: 10.1186/s12885-015-1274-1.
10. Abnous K, Barati B, Mehri S, Farimani MRM, Alibolandi M, Mohammadpour F, *et al.* Synthesis and molecular modeling of six novel monastrol analogues: evaluation of cytotoxicity and kinesin inhibitory activity against HeLa cell line. DARU. 2013;21(1):70-77. DOI: 10.1186/2008-2231-21-70.
11. Guan B, Zhang C, Ning J. EDGA: a population evolution direction-guided genetic algorithm for protein-ligand docking. J Comput Biol. 2016;23(7):585-596. DOI: 10.1089/cmb.2015.0190.
12. Studio D, Insight I. Accelrys Software Inc. San Diego, CA. 2009;92121. https://www.3dsbiovia.com/products/collaborative-science/biovia-discovery-studio/visualization-download.php.
13. Morris GM, Huey R, Olson AJ. Using autodock for ligand-receptor docking. Curr Protoc Bioinformatics. 2008;24(1):8-14. DOI: 10.1002/0471250953.bi0814s24.

14. El-Emary T, Abdel-Mohsen SA. Synthesis and antimicrobial activity of some new 1,3-diphenyl-pyrazoles bearing pyrimidine, pyrimidinethione, thiazolopyrimidine, triazolopyrimidine, thio-and alkylthiotriazolop-yrimidinone moieties at the 4-position. Phosphorus Sulfur Silicon Relat Elem. 2006;181(11):2459-2474.
DOI: 10.1080/10426500600754695.
15. Awadallah FM, Piazza GA, Gary BD, Keeton AB, Canzoneri JC. Synthesis of some dihydropyrimidine-based compounds bearing pyrazoline moiety and evaluation of their antiproliferative activity. Eur J Med Chem. 2013;70:273-279.
DOI: 10.1016/j.ejmech.2013.10.003.
16. Damgaard M, Al-Khawaja A, Nittegaard-Nielsen M, Petersen RF, Wellendorph P, Frølund B. Monastrol, a 3,4-dihydropyrimidin-2(1H)-thione, as structural scaffold for the development of modulators for GHB high-affinity binding sites and $\alpha_1\beta_2\delta$ $GABA_A$ receptors. Eur J Med Chem. 2017;138:300-312.
DOI: 10.1016/j.ejmech.2017.06.024.
17. Banoth S, Boda S, Perugu S, Balabadra S, Manga V. Design, synthesis, biological evaluation and *in silico* molecular docking studies of novel benzochromeno [2,3-d] thiazolopyrimidine derivatives. Res Chem Intermediat. 2018;44(3):1833-1846.
DOI: 10.1007/s11164-017-3201-3.
18. Zhang X, Breslav M, Grimm J, Guan K, Huang A, Liu F, *et al*. A new procedure for preparation of carboxylic acid hydrazides. J Org Chem. 2002;67(26):9471-9474.
DOI: 10.1021/jo026288n.
19. Shamim S, Khan KM, Salar U, Ali F, Lodhi MA, Taha M, *et al*. 5-Acetyl-6-methyl-4-aryl-3,4-dihydropyrimidin-2(1H)-ones: as potent urease inhibitors; synthesis, *in vitro* screening, and molecular modeling study. Bioorg Chem. 2018;76:37-52.
DOI: 10.1016/j.bioorg.2017.10.021.
20. Hussein WM, Fatahala SS, Mohamed ZM, McGeary RP, Schenk G, Ollis DL, *et al*. Synthesis and kinetic testing of tetrahydropyrimidine-2-thione and pyrrole derivatives as inhibitors of the metallo-β-lactamase from *Klebsiella pneumonia* and *Pseudomonas aeruginosa*. Chem Biol Drug Des. 2012;80(4):500-515.
DOI: 10.1111/j.1747-0285.2012.01440.x.
21. Mokale SN, Shinde SS, Elgire RD, Sangshetti JN, Shinde DB. Synthesis and anti-inflammatory activity of some 3-(4,6-disubtituted-2-thioxo-1,2,3,4-tetrahydropyrimidin-5-yl) propanoic acid derivatives. Bioorg Med Chem Lett. 2010;20(15):4424-4426.
DOI: 10.1016/j.bmcl.2010.06.058.
22. Freshney RI. Culture of specific cell types: Wiley Online Library;2005.
DOI: 10.1002/0471747599.cac023.
23. Said MA, Eldehna WM, Ghabbour HA, Kabil MM, Al-shakliah NS, Abdel-Aziz HA. Solvent-free ring cleavage hydrazinolysis of certain Biginelli pyrimidines. J Chem. 2018;2018:6354742,1-6.
DOI: 10.1155/2018/6354742.
24. Al-Masoudi WA, Al-Masoudi NA, Weibert B, Winter R. Synthesis, X-ray structure, *in vitro* HIV and kinesin Eg5 inhibition activities of new arene ruthenium complexes of pyrimidine analogs. J Coord Chem. 2017;70(12):2061-2073.
DOI: 10.1080/00958972.2017.1334259.
25. Kolb S, Mondésert O, Goddard ML, Jullien D, Villoutreix BO, Ducommun B, *et al*. Development of novel thiazolopyrimidines as CDC25B phosphatase inhibitors. ChemMedChem: Chem Enabling Drug Discov. 2009;4(4):633-648.
DOI: 10.1002/cmdc.200800415.
26. Shastin AV, Korotchenko VN, Nenajdenko VG, Balenkova ES. A novel synthetic approach to dichlorostyrenes. Tetrahedron. 2000;56(35):6557-6563.
DOI: 10.1016/S0040-4020(00)00606.
27. Fu Rg, You Qd, Yang L, Wu Wt, Jiang C, Xu Xl. Design, synthesis and bioevaluation of dihydropyrazolo [3,4-b] pyridine and benzo [4,5] imidazo [1,2-a] pyrimidine compounds as dual KSP and Aurora-A kinase inhibitors for anti-cancer agents. Bioorg Med Chem. 2010;18(22):8035-8043.
DOI: 10.1016/j.bmc.2010.09.020.
28. Ragab FA, Abou-Seri SM, Abdel-Aziz SA, Alfayomy AM, Aboelmagd M. Design, synthesis and anticancer activity of new monastrol analogues bearing 1,3,4-oxadiazole moiety. Eur J Med Chem. 2017;138:140-151.
DOI: 10.1016/j.ejmech.2017.06.026.
29. Samundeeswari S, Chougala B, Holiyachi M, Shastri L, Kulkarni M, Dodamani S, *et al*. Design and synthesis of novel phenyl-1,4-beta-carboline-hybrid molecules as potential anticancer agents. Eur J Med Chem. 2017;128:123-139.
DOI: 10.1016/j.ejmech.2017.01.014.
30. Tcherniuk S, van Lis R, Kozielski F, Skoufias DA. Mutations in the human kinesin Eg5 that confer resistance to monastrol and S-trityl-L-cysteine in tumor derived cell lines. Biochem Pharmacol. 2010;79(6):864-872.
DOI: 10.1016/j.bcp.2009.11.001.
31. Maliga Z, Mitchison TJ. Small-molecule and mutational analysis of allosteric Eg5 inhibition by monastrol. BMC Chem Biol. 2006;6:2-10.
DOI: 10.1186/1472-6769-6-2.
32. Yan Y, Sardana V, Xu B, Homnick C, Halczenko W, Buser CA, *et al*. Inhibition of a mitotic motor protein: where, how, and conformational consequences. J Mol Biol. 2004;335(2):547-554.
DOI: 10.1016/j.jmb.2003.10.074.
33. Akhaja TN, Raval JP. 1,3-Dihydro-2H-indol-2-ones derivatives: design, synthesis, *in vitro* antibacterial, antifungal and antitubercular study. Eur J Med Chem. 2011;46(11):5573-5579.
DOI: 10.1016/j.ejmech.2011.09.023.
34. Kappe CO. 100 years of the Biginelli dihydropyrimidine synthesis. Tetrahedron. 1993;49(32):6937-6963.
DOI: 10.1016/S0040-4020(01)87971-0.
35. Pei YY, Li GC, Ran J, Wei FX. Kinesin family member 11 contributes to the progression and prognosis of human breast cancer. Oncol Lett. 2017;14(6):6618-6626.
DOI: 10.3892/ol.2017.7053.